Calcaneal loading during walking and running

VIRGINIA L. GIDDINGS, GARY S. BEAUPRÉ, ROBERT T. WHALEN, and DENNIS R. CARTER

Biomechanical Engineering Division, Mechanical Engineering Department, Stanford University, Stanford, CA; Rehabilitation Research and Development Center, Veterans Affairs Health Care System, Palo Alto, CA; and Life Sciences Division, NASA Ames Research Center, Mountain View, CA

ABSTRACT

GIDDINGS, V. L., G. S. BEAUPRÉ, R. T. WHALEN, and D. R. CARTER. Calcaneal loading during walking and running. *Med. Sci. Sports Exerc.*, Vol. 32, No. 3, pp. 627–634, 2000. **Purpose:** This study of the foot uses experimentally measured kinematic and kinetic data with a numerical model to evaluate *in vivo* calcaneal stresses during walking and running. **Methods:** External ground reaction forces (GRF) and kinematic data were measured during walking and running using cineradiography and force plate measurements. A contact-coupled finite element model of the foot was developed to assess the forces acting on the calcaneus during gait. **Results:** We found that the calculated force-time profiles of the joint contact, ligament, and Achilles tendon forces varied with the time-history curve of the moment about the ankle joint. The model predicted peak talocalcaneal and calcaneocuboid joint loads of 5.4 and 4.2 body weights (BW) during walking and 11.1 and 7.9 BW during running. The maximum predicted Achilles tendon forces were 3.9 and 7.7 BW for walking and running. **Conclusions:** Large magnitude forces and calcaneal stresses are generated late in the stance phase, with maximum loads occurring at ~70% of the stance phase during walking and at ~60% of the stance phase during running, for the gait velocities analyzed. The trajectories of the principal stresses, during both walking and running, corresponded to each other and qualitatively to the calcaneal trabecular architecture. **Key Words:** CALCANEUS, BIOMECHANICAL MODEL, FOOT, BONE REMODELING, FINITE ELEMENT MODEL, JOINT FORCES, BONE FORCES, MUSCLE FORCES, GROUND REACTION FORCE, BONE ADAPTATION

Experimental determination of the ground reaction force (GRF) vector has allowed investigators to characterize the patterns of external load application to the foot during gait; however, the internal musculoskeletal forces that accompany these external loads and the relationship between the two are not as well understood. Better understanding of the internal loads generated by normal daily loading events such as walking and running can further our understanding of the relationship between bone structure and function. The calcaneus has become an important peripheral site for osteoporosis assessment (4,30,36). A model that relates kinetic and kinematic measurements to loads generated in the calcaneus during daily activities could be used to study the contribution of mechanics to bone development and maintenance. In addition, understanding the relationship between gait and force transmission in the foot is essential for devising methods of injury prevention and treatment.

The parameters that characterize the GRF profile for walking and running are largely dependent on gait velocity (1,5,17). During walking, there is an initial small peak in the vertical GRF, generated after ground contact and termed the "impact" peak, followed by a bimodal waveform with peaks ranging from 1.0 to 1.5 body weights (BW) (1,5,34). The profile for running has a more distinct initial impact peak, usually followed by a single maximum peak achieved at mid stance, ranging from 2.0 to 3.5 BW (5,9,20,34). Measurement of the GRF has been used extensively to evaluate causal factors for gait related injuries; however, the relationship between foot kinematics and kinetics and the resulting stresses in ligaments, joints, and bones is still unknown.

Invasive *in vivo* studies provide valuable information for validation of numerical models but are of limited practicality because they are difficult to perform and raise ethical questions. Computational modeling provides an alternative to *in vivo* experiments. Numerous biomechanical models have been developed to examine muscle forces during quasi-static walking and running (6,23,27–29,31). The objectives of these models are to solve the indeterminacy problem

0195-9131/00/3203-0627/0
MEDICINE & SCIENCE IN SPORTS & EXERCISE®

Submitted for publication April 1998.
Accepted for publication July 1999.

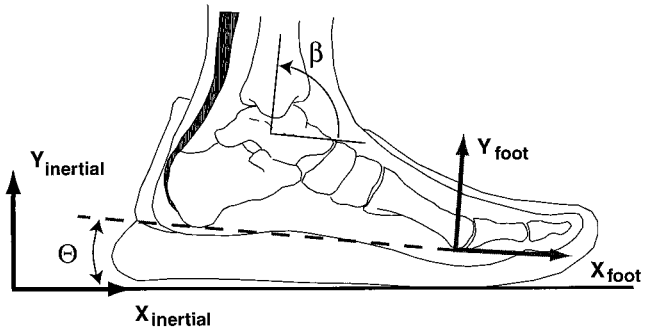

Figure 1—Schematic of the foot as seen in the cineradiographic images. The inertial frame is on the force plate, and the foot reference frame is defined in the sagittal plane by a line drawn from the head of the first metatarsal to the base of the calcaneus. Note that, because of the raised insole at the hindfoot, the foot frame has a small positive angle (θ) when the shoe is flat on the ground.

associated with the large number of unknown parameters and to estimate the internal loading. Seireg and Arvikar (28) utilized minimization of muscle forces and joint moments to solve for muscle and joint reaction forces in the lower extremity during walking. They found that the predicted muscle and joint reaction forces correlated with EMG data. Equilibrium methods have been applied to study the forces in the foot both during walking (23,29,31) and running (6,27). Procter and Paul (23) focused their analysis on the ankle joint, looking at the joint reaction and muscle/tendon forces during walking. They grouped muscles and weighted the forces based on the average tendon cross-sectional area. Scott and Winter (27) divided the lower leg into four static systems, using equilibrium methods to solve for muscle and ankle joint loads during running. Although all of these analyses provide information regarding the loading in and around the ankle joint, none offer a comprehensive analysis that includes an examination of the bone stresses.

Several finite element (FEM) models have been developed to examine the stress patterns in the calcaneus during loading (14,21,37). One of the main difficulties of constructing a FEM model of a biological structure is determining the physiological loading and constraining the structure without imposing nonphysiologic boundary conditions. Yettram and Camilleri (37) used an optimization routine to determine the loading on a two-dimensional FEM model of the calcaneus during static standing. They found qualitative agreement between the resulting stress trajectories and the orientation of apatite crystals in the calcaneus. Oxnard (21) and Hsu (14) examined the stress patterns in the calcaneus at three periods of the stance phase of walking: heel-strike, mid stance, and toe-off. Based on the similarity between the patterns of von Mises stress in the calcaneal models and the distribution of areal densities in the mid-sagittal plane, Hsu concluded that the patterns formed by the trabeculae in the calcaneus are predominantly influenced by the forces and the stresses induced during the toe-off phase of walking or running. Although this work represents an important first effort at numerical modeling of the calcaneus, it does have three limitations: 1) the loads applied to the calcaneus were assumed from the predictions of several different numerical models, thereby combining estimates of loading that do not guarantee equilibrium; 2) the displacement constraint across the calcaneocuboid joint, which enforces static equilibrium, results in stress artifacts and nonphysiologic tensile joint reaction forces; and 3) foot kinematics were not considered when determining the lines of action of muscle forces, ligament forces, joint distributed loads, or the GRF. Additionally, none of the FEM analyses performed to date examine the loading that occurs during running or present a methodology that couples kinematic and kinetic experimental data for evaluating calcaneal loading throughout the gait cycle.

The purpose of the present study was to develop a model of the calcaneus that does not require *a priori* assumptions regarding applied loads and joint pressures. This model was used to examine the loading on the calcaneus throughout the

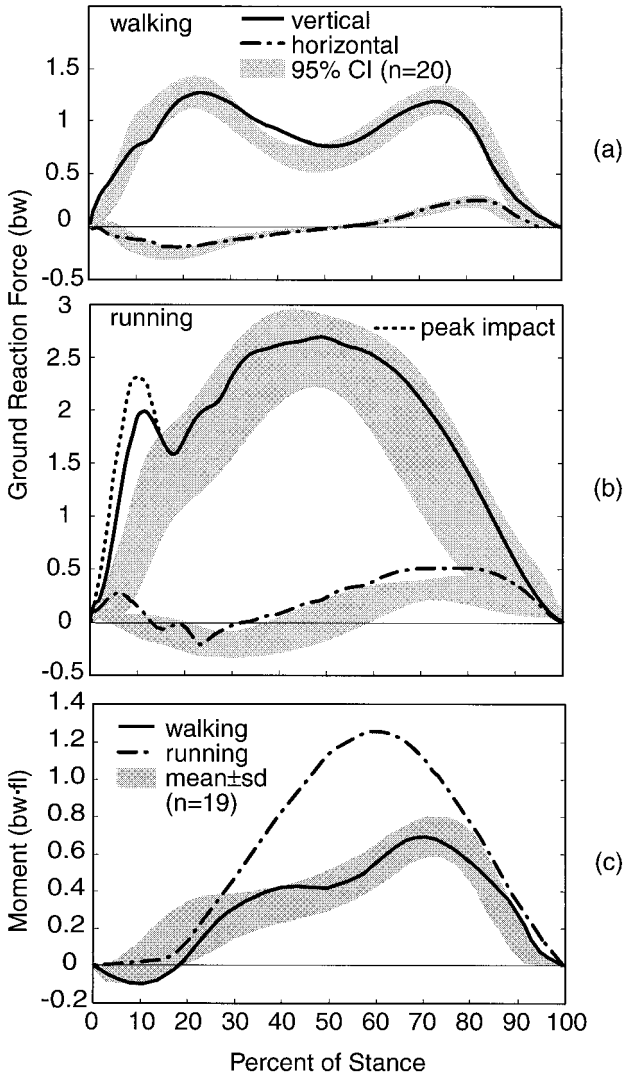

Figure 2—Experimentally determined horizontal and vertical components of the ground reaction force for walking (a) and running (b), and the resulting moment about the ankle joint (c). All force data were normalized by body weight and all distance measurements were normalized by foot length. Shaded regions of (a) and (b) are normative data (95% confidence interval) from 20 male subjects walking (1.62 ± 0.04 m·s^{-1}, N = 20) (± 1 SD) and running (3.70 ± 0.21 m·s^{-1}, N = 20) at similar speeds (5). Shaded region of (c) is ± 1 SD (1.4 m·s^{-1}) (34).

TABLE 1. Results for kinetic and kinematic varibles are shown including β and θ, the ankle flexion, and foot-ground angles. Parameters from the FEM analysis are the GRF transformed to the foot frame, ankle moment, the GRF moment arm, R and the Achilles tendon moment arm, r.

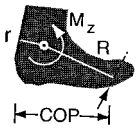

	Walking						Running				
	impact	20%	40%	60%	70%	80%	impact	20%	40%	60%	80%
Cineradiography results											
COP (fl)	0.11	0.34	0.73	0.85	0.89	0.95	0.28	0.42	0.68	0.81	0.91
Inertial frame											
F_x (BW)	−0.09	−0.15	−0.03	0.08	0.22	0.27	−0.05	−0.07	0.05	0.42	0.51
F_y (BW)	0.75	1.24	0.89	0.93	1.17	0.93	1.52	1.60	2.53	2.45	1.23
FEM model parameters											
Foot frame											
F_x (BW)	−0.09	−0.30	−0.24	−0.33	−0.48	−0.48	−0.13	−0.26	−0.48	−0.31	−0.19
F_y (BW)	0.75	1.21	0.86	0.88	1.08	0.84	1.51	1.57	2.49	2.47	1.31
R (fl)	0.11	0.0	0.42	0.50	0.50	0.50	0.014	0.06	0.30	0.48	0.60
M_z (BW·fl)	−0.082[a]	0.0	0.38	0.47	0.60	0.48	0.02	0.09	0.75	1.2	0.8
r = 0.20 fl											

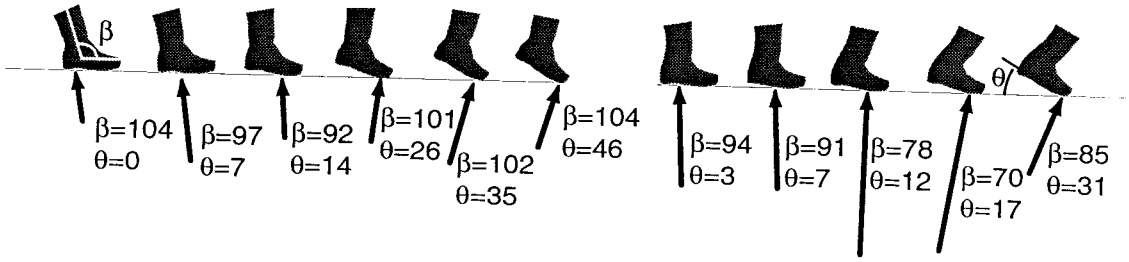

COP, center of pressure; F_x, horizontal reaction force; F_y, vertical reaction force; M_z, moment about the ankle joint.
[a] The Achilles tendon is slack at impact.

gait cycle for both walking and running using externally measured ground reaction forces and high speed cineradiography, to capture the positions of the skeletal structures directly in relation to the ground reaction force, as input into the model. The goal of this analysis was to evaluate the contribution of different loading events on the resulting joint contact forces, ligament and tendon loads, and bone stresses.

MATERIALS AND METHODS

Kinematic and kinetic data were determined for a normal subject during walking and running using cineradiography and force plate gait measurements. Data were acquired from one male subject (weight 675 N, height 1.73 m, and foot length 0.24 m). Institutional approval was obtained for the human subjects protocol and the subject signed an informed consent before participating. Total x-ray exposure was limited to 400 mR total entrance skin (foot/ankle) exposure (4-mR whole-body dose). The x-ray tube was mounted perpendicular to the raised runway adjacent to the force platform. Sagittal plane x-ray images were sampled at 1000 Hz concurrent with sampling of the ground reaction force vector at 2000 Hz (Figs. 1 and 2). Metal reference markers, attached to the force plate and visible in each x-ray image, allowed us to transform GRF and center of pressure (COP) data from the force plate reference frame to the image and foot reference frames. Kinematic data, including foot-ground angle (θ) and ankle dorsi/plantar flexion angle (β) (Fig. 1), were measured from the cineradiographic images using the public domain NIH image program (developed at the U.S. NIH and available on the Internet at http://rsb.info.nih.gov). Segments were defined from the bony landmarks as: 1) tibial axis and 2) axis intersecting the plantar surface of the metatarsal head and the calcaneal tuberosity. The center of rotation (COR) of the ankle was assumed to be fixed and was determined from the x-ray image as the intersection of a set of radial rays normal to the tibiotalar joint curvature. The moment about the ankle joint was calculated from the vertical and fore/aft components of the GRF, the COP data, and the location of the COR with respect to the COP (Fig. 2). The subject's gait velocity was 1.62 $m \cdot s^{-1}$ during the walking trial and 3.71 $m \cdot s^{-1}$ during the running trial.

Toward the dual goal of developing a scalable subject-specific calcaneus/foot model and examining size-independent loading of the calcaneus, we have nondimensionalized GRFs by normalizing to BW and linear dimensions to foot length (fl). The moment arm of the Achilles tendon (r), normalized to the foot length, was measured in each image as the perpendicular distance from the COR to the Achilles tendon. From this measurement, a mean value of 0.20 fl was calculated and used in the FEM model. The moment arm of the GRF (R) was measured from the COR to the line of action of the resultant GRF (vertical and fore/aft components only) passing through the COP. The subject's kinematic and kinetic data from this analysis, evaluated at discrete time points during stance, were used for input into the FEM model (Table 1).

Model development. A contact-coupled approach was used to model the calcaneus with the inclusion of the hindfoot and forefoot. A contact-coupled formulation is a method of FEM modeling where the interaction between two objects is modeled as a contact surface, over which sliding or separation can occur, and the stress states in both objects are solved

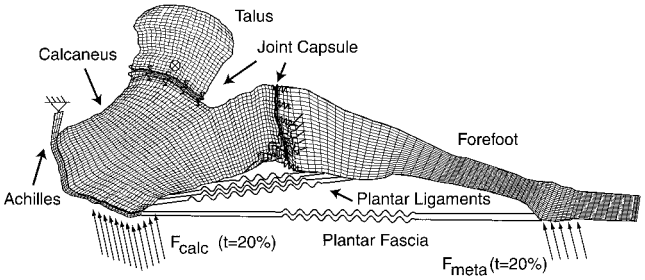

Figure 3—The FEM model with boundary conditions shown at 20% of stance during walking. Loads were applied at two locations: the calcaneus (F_{calc}) and the metatarsal head (F_{meta}). Displacement boundary conditions ($u_x = 0$, $u_y = 0$) were assigned at the end of the Achilles tendon and in the center of the talar body, in the location of the COR of the ankle.

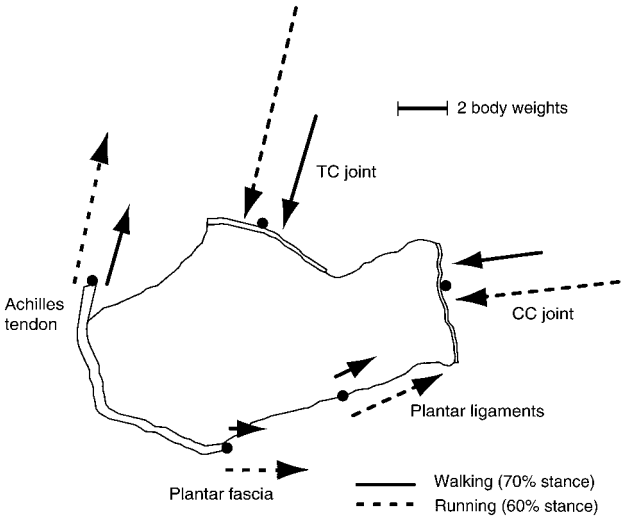

Figure 4—Diagram of the calcaneus showing ligament, tendon, and joint forces acting on the calcaneus at 70% of stance during walking and 60% of stance during running. Vectors are shown slightly offset from the location of force application, indicated by a dot. Predicted TC and CC joint capsule loads at peak loading were small in magnitude and are not shown.

simultaneously. The pressure distribution across joints in contact-coupled models is calculated based on the interaction between the two bodies under the applied loads. The method is computationally expensive because it is inherently nonlinear, but it can reduce the uncertainties caused by assuming pressure distributions across joint surfaces.

The geometry for the 2-D numerical model was created from a mid-sagittal CT scan of a foot. Outer contours of the talus, calcaneus and the forefoot, including the cuboid and the metatarsals, were obtained using an edge detection algorithm and used as a basis for constructing the FEM mesh (XYZ Scientific Applications, Livermore, CA) (Fig. 3). The three bone structures; the talus, the calcaneus and the forefoot; and the Achilles tendon were modeled using bilinear plane strain elements, with an out-of-plane thickness of 35 mm (0.15 fl). Two frictionless contact surfaces were defined, the first between the talus and calcaneus in the location of the talocalcaneal joint (TC) and the second between the calcaneus and the cuboid representing the calcaneocuboid joint (CC). The articulating surfaces of each bone were covered by cartilage elements. The contact interfaces allowed for arbitrary contact, sliding and separation between the deformable bodies.

Several assumptions were made regarding the muscle activity about the ankle joint. The action of the tibialis anterior muscle was included in the model in the case where a negative moment was generated about the ankle, at the time of heel strike during walking, but otherwise co-contraction of the dorsiflexor muscles was neglected. EMG data has shown that tibialis anterior muscle is active before and after the stance phase of gait, but is not activated during stance (22). It was also assumed that all plantar flexion occurred by contraction of the triceps surae muscle group. Although other plantar flexors are active during gait (3), it is generally agreed that their contribution to the flexion moment is small. The soleus and gastrocnemius together account for 93% of the plantar flexion torque during normal gait (22). Including additional plantar flexors to the model could increase compression across the plantar surface of the foot, modestly reducing the magnitude of the ligament forces.

Soft tissues constraining foot motion, including the joint capsules, short plantar ligament, long plantar ligament, and the plantar fascia were modeled using tension-only linear spring elements. Placement of the soft tissue structures was determined from anatomical landmarks and studies of the foot (26,32). The force-displacement relationship of each ligament and the plantar fascia was computed as the product of its respective cross-sectional area and the tissue elastic modulus, divided by its unstretched length.

The material properties used in the model were assumed to be linear elastic, isotropic and homogeneous. The calcaneus was assigned a uniform modulus of 5,000 MPA and a Poisson's ratio of 0.32, representing very dense trabecular bone. The talus and the forefoot were assigned a modulus 15,000 MPa and a Poisson's ratio of 0.32, consistent with values for cortical bone. The material properties of the ligaments and the cartilage were obtained from the literature (Table 2) (2,12,13,35). The model was constrained to have zero displacement at the proximal end of the Achilles tendon, determined from the CT image, and at the assumed COR of the ankle joint. The model consisted of 4327 elements with 8468 degrees of freedom, including the Lagrange multipliers needed to solve the contact problem.

We distributed the GRF on the foot model based on foot kinematics and the location of the COP data from the cineradiographic study. To solve for ligament and tendon forces, joint contact forces and bone stresses, it was necessary to dimension the model and apply forces in their true magnitudes using the scale factors from Table 1. After the analysis, all forces were renormalized with the results reported in body weights. Distributed loads were assigned at

TABLE 2. Material properties of the ligaments and cartilage.

	E (MPa)	ν
Achilles	800	0.42
Cartilage	12.0	0.42
Plantar fascia	350	0.42
Plantar ligaments	500	0.42

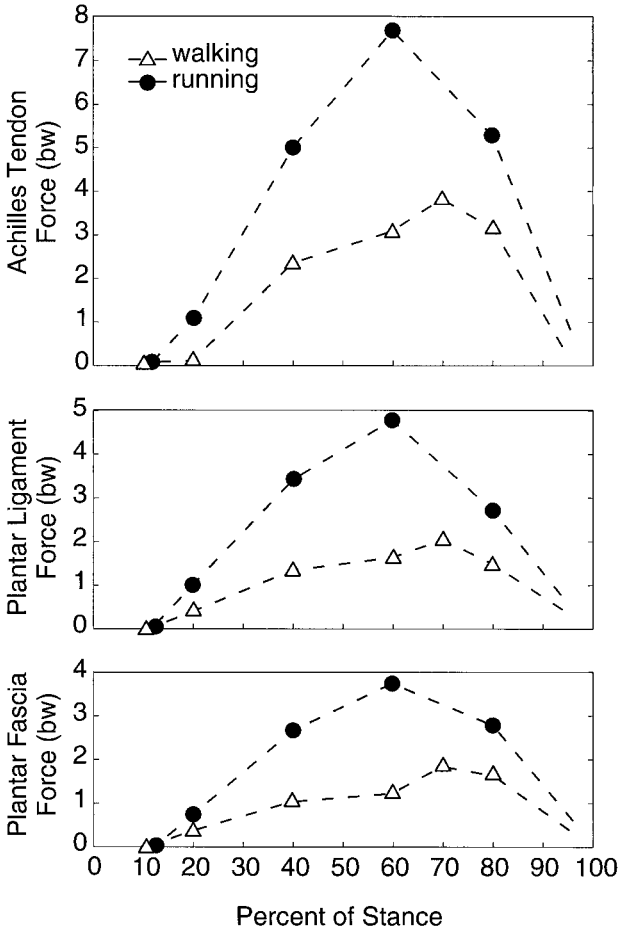

Figure 5—Force in the Achilles tendon, plantar ligaments, and plantar fascia as predicted by the FEM model during walking, running, and high-impact running.

two locations, at the base of calcaneus and at the metatarsal head, to simulate the GRF acting on the foot. The magnitudes of the forces applied at each of the two locations were weighted based on the location of the COP and the magnitude of the GRF. The GRF was transformed from the inertial reference frame to a foot reference frame for application to the FEM model (Table 1). This method of load application applies the total force exerted on the external surface of the shoe directly to the foot and does not incorporate the possible effects of load redistribution which may play some role in the mechanics of load transfer from the shoe to the foot early in the gait cycle when the heel is on the ground.

The FEM model was solved using nonlinear geometry, large strain and finite sliding theory (ABAQUS 5.5, Hibbitt, Karlsson & Sorensen, Inc., Pawtucket, RI). The analysis was performed quasi-statically with boundary conditions corresponding to the initial impact peak, 20, 40, 60, 70 (walking only), and 80% of the stance phase of walking and running. The analysis was performed at 70% of walking to evaluate the calcaneal loading at the temporal occurrence of maximal ankle moment. The influence of high initial impact peak was investigated by applying the maximum impact measured by Munro et al. (20) during running. Total loads across the TC and CC joint surfaces were computed by summing the force transmitted across the contact surfaces in the model. Ligament and tendon forces were calculated by summing the force transmitted across these structures throughout the gait cycle.

During the gait cycle, as loads applied to the calcaneus create deformations, the energy is stored in the form of elastic strain energy (SE). Strain energy has been used as a stimulus driving bone adaptation in remodeling simulations (8,11,15). The total elastic SE in a bone provides a gross measure of the stimulus the bone receives from a load event. By examining differences in total SE occurring during the step cycle, it is possible to evaluate the relative importance, in terms of stimulus to the bone, of the different loading configurations that occur during one step. The results of the analysis for total SE in the calcaneus were normalized by the maximum SE occurring during running, resulting in a scale from 0 to 1 of normalized SE values during gait.

RESULTS

The total joint contact, Achilles tendon, and plantar fascia and plantar ligament forces all contribute to the loads on the calcaneus during gait. Examining a diagram of the forces acting on the calcaneus, at 70% of stance for walking and 60% of stance for running, reveals how these forces contribute to the equilibrium configuration (Fig. 4). The Achilles tendon and plantar fascia and plantar ligaments show similar patterns of force development, with peaks for walking and running occurring at 70% and 60% of stance (Fig. 5). The model predicts peak loads for the Achilles tendon of 3.9 BW during walking and 7.7 BW during running. The

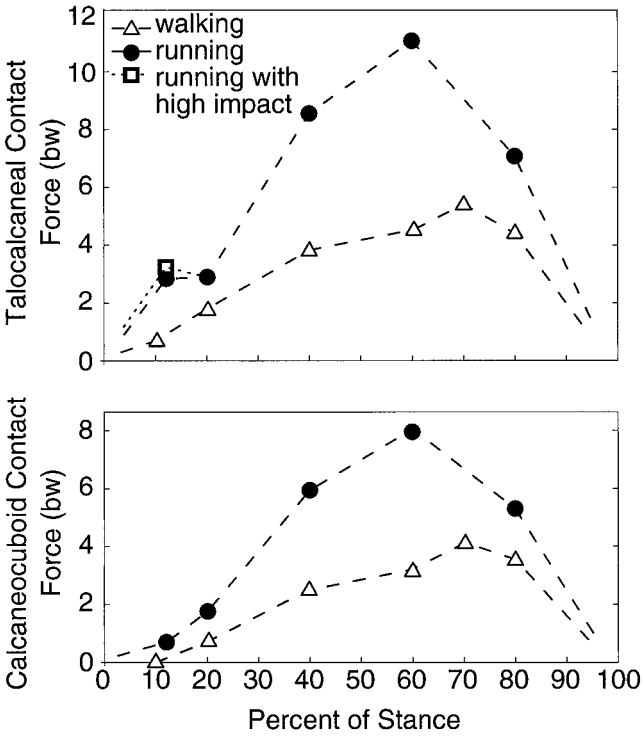

Figure 6—Resultant forces across the talocalcaneal and calcaneocuboid joints as predicted by the FEM model during walking, running, and high-impact running.

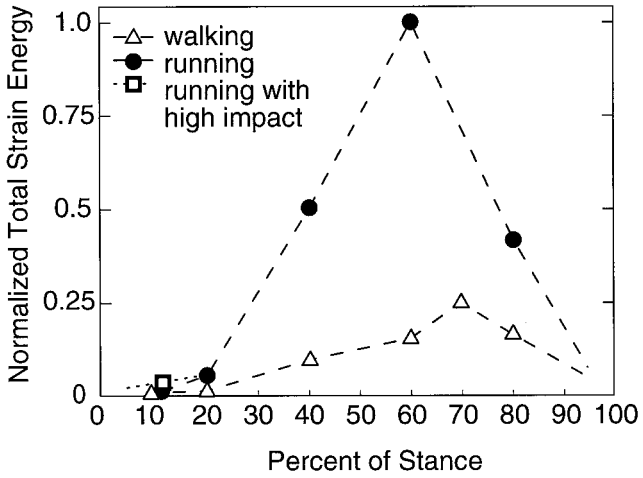

Figure 7—Model predictions of total strain energy in the calcaneus during walking, running, and high-impact running.

loads in the plantar fascia and the plantar ligaments have peak load magnitudes of 1.8 and 2.2 BW during walking and 3.7 and 4.8 BW during running, respectively. Ligament and tendon forces predicted using the high-impact model do not differ appreciably from those predicted at impact during "normal" running.

The model predicts that the total contact force across the TC joint reaches maximum values of 5.4 BW during walking and 11.1 BW during running (Fig. 6). Across the CC joint, maximum loads are 4.2 and 7.9 BW, for walking and running (Fig. 6). For both joints, the peaks occur at 70% of stance for walking and at 60% of stance for running. Slightly elevated TC joint loading of 3.1 BW is observed for the high impact load.

Maximum total strain energy is stored in the calcaneus during walking at 70% of stance and during running at 60% of stance (Fig. 7). The maximum SE during walking is 25% of the peak calcaneal SE during running.

The compressive principal stress trajectories extend from the subtalar joint surface posterior to the insertion of the Achilles tendon and anterior toward the superior surface of the calcaneocuboid joint (Fig. 8a). Tensile trajectories extend along the inferior aspect of the calcaneus (Fig. 8b). A 20-mm thick sagittal CT scan section of the calcaneus and a 3.5-mm thick histologic section illustrate the correspondence between bone architecture and the principal stress trajectories (Fig. 8c and 8d).

DISCUSSION

This study demonstrates that the magnitude of loading in the hindfoot increases throughout the gait cycle, peaking in the later portion of stance. The shape of the force-time curve for all of the variables examined in this study corresponds qualitatively with the moment about the ankle joint, which is calculated from the external GRF. As the moment arm of the GRF, extending from the center of rotation of the ankle to the location of the center of pressure, increases during gait, the moment increases, which is balanced internally by the force in the Achilles tendon. Comparison of the results for walking versus those for running show that the peak ligament and tendon forces during running are scaled from those during walking by a factor of two at the two gait speeds analyzed. This corresponds to the scale factor, for these trials, of the peak moments about the ankle joint.

Low-magnitude loading during the early stance phase suggests that the vertical impact peak does not play an important role in stress generation in the calcaneus. The results for the high-impact case show only slight increases in the talocalcaneal joint contact force magnitudes early in the gait cycle. For the kinematic data analyzed, the impact peak occurs as the line of action of the GRF passes close to the center of the ankle joint, resulting in only small magnitude moments being generated about the ankle joint. Increasing the magnitude of the GRF during this portion of gait only increases the TC joint load, with no effect on the other loads evaluated in the model. The exact etiology of injuries to the foot during gait, and during running in particular, is unknown, making it difficult to conclude that this portion of gait is insignificant. However, if the likelihood of injury is related to force magnitude, then the greatest potential for injury is during mid-to-late stance when maximal calcaneal loading occurs, as has been suggested by Scott and Winter (27).

The results demonstrated quantitative agreement with previous numerical models and *in vivo* measurements. During running, the model of Scott and Winter (27) found peak Achilles tendon loads of 6.1–8.2 BW, ankle compressive joint loads of 10.3–14.1 BW, and plantar fascial loads of 1.3–2.9 BW, with the maximum values occurring in late mid stance, compared with our model predictions of 7.7, 11.1, and 3.7 BW, respectively. Komi (18) measured the force in the Achilles tendon *in vivo* during walking and running. From a curve fit of his data relating running velocity to Achilles tendon force, we found that our model prediction of 7.7 BW closely agrees with the experimental result of 7.5 BW. Additionally, the patterns of loading throughout the stance phase of gait predicted by our model agree with the

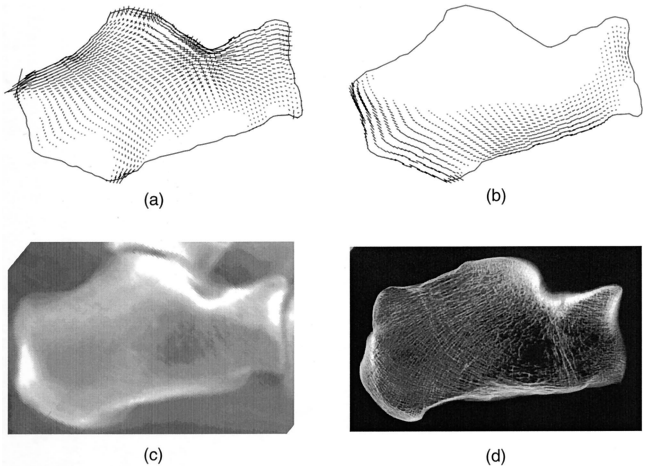

Figure 8—Compressive (a) and tensile (b) principal stress trajectories, sagittal CT scan (c), and histologic section (d). Principal stress trajectories shown are from 70% of the stance phase of walking but are typical of those seen throughout the step cycles of both walking and running.

in vivo force profile in the Achilles tendon during both walking and running (18).

The results suggest that the load conditions at late mid stance, 70% for walking and 60% for running, will provide the largest and perhaps most influential stimulus to the bone tissue during the gait cycle. This result may be somewhat approximate due to the relatively low number of sampling points used in our analysis. Based on these results, we would expect that bone remodeling simulations would be able to predict many of the bone morphological features based on the application of the peak-load case alone. The peak SE for running was four times that for walking, suggesting that calcaneal bone density in runners would be much higher than in a nonrunning population. Whalen et al. (33) hypothesized that stress magnitudes have a greater influence on bone mass than the number of cycles of loading. Although the number of running cycles per day for a typical runner is much less than the number of walking cycles, the running cycles, due to the large magnitude SE, could be influential in determining the bone mass or density distribution.

The internal architecture of the calcaneus is a complex arrangement of distinct systems of trabeculae with a triangular zone of low density bone at the center of these systems (Fig. 8c and 8d). Trabecular systems extend from the subtalar surface toward the distal heel and anterior toward the superior aspect of the CC joint. Trabeculae also extend along the bottom surface of the calcaneus. The principal stress trajectories correspond to these three distinct systems of trabeculae, with compressive trajectories extending posteriorly and anteriorly along the superior half of the calcaneus and the tensile trajectories extending along the inferior half. There are variations in the magnitudes of the stresses throughout the gait cycle and between walking and running, but there are only small variations in the directions of the principal stress trajectories.

The geometry of the calcaneal model was represented in the mid-sagittal plane and did not consider the effect of out-of-plane loading. Because locomotion is primarily forward motion, we would expect that the majority of muscle and soft tissue action is in the plane of progression of the body during walking. Eng and Winter (10) performed a three-dimensional kinematic analysis of the lower limbs and determined that the magnitude of the sagittal plane moment was $>$ 10 times that of the moments generated in the frontal and transverse planes and that 93% of the work performed at the ankle joint occurred in the sagittal plane. These results indicate that modeling the calcaneus in the sagittal plane is a reasonable assumption in terms of the directions of major load application.

We assumed that the center of rotation of the ankle joint and the end of the Achilles tendon were fixed, modeling the ankle joint as a single degree-of-freedom hinge. The extent to which the COR of the ankle joint translates during normal gait is still a subject of some debate. Anthropometric data suggests that the talocrural joint can be considered to be a single-axis joint (16), although *in vivo* kinematic analysis suggests that the COR does move somewhat within the sagittal plane during weight-bearing activities (25). *In vivo* magnetic resonance imaging (MRI) imaging (24) of ankle motion demonstrated a significant increase in the Achilles tendon moment arm and small variations in the location of the COR within the talar body during passive plantarflexion from 100 to 150 degrees; however, within the range of normal ankle flexion during stance (60° in dorsiflexion to 110° in plantarflexion (19)), the study of Rugg et al. (24) did not show significant changes in the tendon moment arm length or the location of the COR. Carrier et al. (7) examined the relationship between muscle and GRF moment arms in the foot and found that the change of the Achilles moment arm during stance, of less than 15%, is insignificant relative to the change in the moment arm of the GRF, which changes by as much as a factor of 20. Given the existing information regarding the location of the COR and the change in the Achilles tendon moment arm during gait, fixing both of these for the analysis is a reasonable approximation.

In the present study, we have developed a two-dimensional contact-coupled model of the foot that incorporates experimentally measured kinetic and kinematic data to examine the internal loading of the foot during walking and running. This biomechanical model allowed for direct application of the external ground reaction force, such that *a priori* assumptions regarding the calcaneal boundary conditions were not needed. This work represents an important first step in understanding the loading on the calcaneus, how loads vary during the gait cycle, and the resulting stress distributions within the calcaneus. This work is not only valuable to the field of foot mechanics, providing insight into the relationship between external loading and internal force generation in the foot, but is also of value to the study of functional bone adaptation, providing a model that can be applied clinically to examine the relationship between activities loading the foot and the generation of bone stresses.

We thank Scott Tashman for his collaboration on the gait analysis and for the use of his lab. We also thank Chye Yan and Cliff Les for their assistance.

This work was supported by the American Association of University Women, Veterans Affairs grants (B802-RA and A501–3RA), and NASA (NCC2–5121).

Address for correspondence: Virginia Giddings, Exponent Failure Analysis Associates, 149 Commonwealth Drive, Menlo Park, CA 94025. E-mail: vgiddings@exponent.com.

REFERENCES

1. Andriacchi, T. P., J. A. Ogle, and J. O. Galante. Walking speed as a basis for normal and abnormal gait measurements. *J. Biomech.* 10:261–268, 1977.
2. Attarian, D. E., H. J. McCrackin, D. P. Devito, J. H. McElhaney, and W. E. Garrett, Jr. Biomechanical characteristics of human ankle ligaments. *Foot Ankle* 6:54–58, 1985.
3. Basmajian, J., and G. Stecko. The role of muscles in arch support of the foot. *J. Bone Joint Surg.* 45A:1184–1190, 1963.
4. Black, D. M., S. R. Cummings, H. K. Genant, M. C. Nevitt, L. Palermo, and W. Browner. Axial and appendicular bone density predict fractures in older women. *J. Bone Miner. Res.* 7:633–638, 1992.

5. BREIT, G. A., and R. T. WHALEN. Prediction of human gait parameters from temporal measures of foot- ground contact. *Med. Sci. Sports Exerc.* 29:540–547, 1997.
6. BURDETT, R. Forces predicted at the ankle during running. *Med. Sci. Sports Exerc.* 14:308–316, 1982.
7. CARRIER, D. R., N. C. HEGLUND, and K. D. EARLS. Variable gearing during locomotion in the human musculoskeletal system. *Science* 265:651–653, 1994.
8. CARTER, D. R., D. P. FYHRIE, and R. T. WHALEN. Trabecular bone density and loading history: regulation of connective tissue biology by mechanical energy. *J. Biomech.* 20:785–794, 1987.
9. CAVANAGH, P. R., and M. A. LAFORTUNE. Ground reaction forces in distance running. *J. Biomech.* 13:397–406, 1980.
10. ENG, J. J., and D. A. WINTER. Kinetic analysis of the lower limbs during walking: what information can be gained from a three-dimensional model? *J. Biomech.* 28:753–758, 1995.
11. FYHRIE, D. P., and D. R. CARTER. A unifying principle relating stress to trabecular bone morphology. *J. Orthop. Res.* 4:304–317, 1986.
12. GIBBONS, D. Biomedical materials. In: *Handbook of Engineering in Medicine, and Biology*, D. Fleming and B. Feinberg (Eds.). Cleveland: CRC Press, 1976, pp. 254.
13. HAYES, W. C., and L. F. MOCKROS. Viscoelastic properties of human articular cartilage. *J. Appl. Physiol.* 31:562–568, 1971.
14. HSU, A.-T. Trabecular architecture and finite element analysis of the human calcaneus. In: *Physical Therapy*. Los Angeles: University of Southern California, 1989, pp. 1–250.
15. HUISKES, R., H. WEINANS, H. J. GROOTENBOER, M. DALSTRA, B. FUDALA, and T. J. SLOOFF. Adaptive bone-remodeling theory applied to prosthetic-design analysis. *J. Biomech.* 20:1135–1150, 1987.
16. ISMAN, R., and V. INMAN. Anthropometric studies of the human foot and ankle. *Bull. Prostet. Res.* 10-11:97–129, 1969.
17. KELLER, T., A. WEISBERGER, J. RAY, S. HASAN, R. SHIAVI, and D. SPENGLER. Relationship between vertical ground reaction force and speed during walking, slow jogging, and running. *Clin. Biomech.* 11:253–259, 1996.
18. KOMI, P. V. Relevance of *in vivo* force measurements to human biomechanics. *J. Biomech.* 23(Suppl. 1):23–34, 1990.
19. MANN, R. Biomechanics of running, In: *AAOS Symposium on the Foot and Leg in Running Sports*, Coronado, CA, September 1980, R. P. Mack (Ed.). St. Louis, MO: C.V. Mosby, 1982, pp. 1–29.
20. MUNRO, C. F., D. I. MILLER, and A. J. FUGLEVAND. Ground reaction forces in running: a reexamination. *J. Biomech.* 20:147–155, 1987.
21. OXNARD, C. E. Bone and bones, architecture and stress, fossils and osteoporosis. *J. Biomech.* 26(Suppl. 1):63–79, 1993.
22. PERRY, J. *Gait Analysis -Normal, and Pathological Function.* Thorofare, NJ: Slack, Inc., 1992, pp. 51–87.
23. PROCTER, P., and J. P. PAUL. Ankle joint biomechanics. *J. Biomech.* 15:627–634, 1982.
24. RUGG, S. G., R. J. GREGOR, B. R. MANDELBAUM, and L. CHIU. *In vivo* moment arm calculations at the ankle using MRI. *J. Biomech.* 23:495–501, 1990.
25. SAMMARCO, G. J., A. H. BURSTEIN, and V. H. FRANKEL. Biomechanics of the ankle: a kinematic study. *Orthop. Clin. North Am.* 4:75–96, 1973.
26. SARRAFIAN, S. *Anatomy of the Foot, and Ankle. Descriptive, Topographic, Functional.* Philadelphia: JB Lippincott, 1983, pp.1–433.
27. SCOTT, S. H., and D. A. WINTER. Internal forces of chronic running injury sites. *Med. Sci. Sports Exerc.* 22:357–369, 1990.
28. SEIREG, A., and R. J. ARVIKAR. A mathematical model for evaluation of forces in lower extremities of the musculo-skeletal system. *J. Biomech.* 6:313–326, 1973.
29. STAUFFER, R., E. CHAO, and R. BREWSTER. Force and motion analysis of the normal, diseased, and prothetic ankle joint. *Clin. Orthop. Rel. Res.* 127:189–196, 1977.
30. TURNER, C. H., M. PEACOCK, L. TIMMERMAN, J. M. NEAL, and C. C. JOHNSON, JR. Calcaneal ultrasonic measurements discriminate hip fracture independently of bone mass. *Osteoporos. Int.* 5:130–135, 1995.
31. VERES, G. Graphic analysis of forces acting upon a simplified model of the foot. *Prosthet. Orthot. Int.* 1:161–172, 1977.
32. WARD, K., and R. SOAMES. Morphology of the plantar calcaneocuboid ligaments. *Foot Ankle Int.* 18:649–653, 1997.
33. WHALEN, R. T., D. R. CARTER, and C. R. STEELE. Influence of physical activity on the regulation of bone density. *J. Biomech.* 21:825–837, 1988.
34. WINTER, D. A. *The Biomechanics, and Motor Control of Human Gait.* Waterloo, Ontario: University of Waterloo Press, 1987, pp. 1–296.
35. WRIGHT, D., and D. RENNELS. A study of the elastic properties of plantar fascia. *J. Bone Joint Surg.* 46A:482–492, 1964.
36. YAMADA, M., M. ITO, K. HAYASHI, M. OHKI, and T. NAKAMURA. Dual energy X-ray absorptiometry of the calcaneus: comparison with other techniques to assess bone density and value in predicting risk of spine fracture. *Am. J. Roentgenol.* 163:1435–1440, 1994.
37. YETTRAM, A. L., and N. N. CAMILLERI. The forces acting on the human calcaneus. *J. Biomed. Eng.* 15:46–50, 1993.